Journal of Applied Geophysics 109 (2014) 242–255

Contents lists available at ScienceDirect

Journal of Applied Geophysics

journal homepage: www.elsevier.com/locate/jappgeo

Remanence, self-demagnetization and their ramifications for magnetic modelling of iron oxide copper-gold deposits: An example from Candelaria, Chile

James Austin [a,*], Silvana Geuna [b], David Clark [a,c], Dean Hillan [a,1]

[a] CSIRO Earth Science and Resource Engineering, North Ryde, Australia
[b] Departamento de Ciencias Geológicas, Universidad de Buenos Aires, Argentina
[c] CSIRO Materials Science and Engineering, Lindfield, Australia

ARTICLE INFO

Article history:
Received 31 October 2013
Accepted 5 August 2014
Available online 12 August 2014

Keywords:
Magnetic modelling
Iron oxide copper-gold (IOCG)
Magnetite
Magnetic susceptibility
Remanent magnetization
Self-demagnetization

ABSTRACT

Magnetic modelling can be a powerful tool for understanding the architecture of numerous types of mineralized systems; e.g., iron ore, IOCG and porphyry deposits. In such modelling, the induced component is generally assumed to be dominant, whereas remanent magnetization is often neglected and, furthermore, the effects of self-demagnetization are commonly ignored. We present rock property measurements (magnetic susceptibility and remanent magnetization) from the Candelaria IOCG deposit in northern Chile. The results demonstrate that remanence is relatively weak (<20% of induced) and that the causative lithologies have very high magnetic susceptibilities (3–4 SI), which makes them highly prone to self-demagnetization. The rock property results were used to constrain a simplified forward model in which the causative bodies are modelled as a series of sub-horizontal highly magnetic sheets, corresponding to "mantos". These "mantos" occur north and south of Candelaria, sub-perpendicular to a splay off the Atacama Fault Zone. We demonstrate that Candelaria's unusual magnetic anomaly is due to a combination of its highly magnetic sub-horizontal architecture, and self-demagnetization effects. A further simplified model was used to calculate two synthetic anomalies, one ignoring and the other incorporating the self-demagnetization effect. These synthetic anomalies demonstrate that the magnetic anomaly amplitude is suppressed by up to approximately 50% at Candelaria due to self-demagnetization, and that the induced magnetization is also slightly rotated from the regional inducing field towards the plane of the "mantos". The dominant paleomagnetic component recorded by the Candelaria deposit and host rocks is a normal polarity remanence of moderate to high stability which is interpreted to have been acquired during the mid-Cretaceous alteration and mineralisation event(s) that generated the magnetic minerals (predominantly magnetite). However, the presence of a reversed polarity overprint component in some samples suggests that the Candelaria deposit and its immediate environs have experienced a post 83 Ma thermal or thermochemical event that has not been previously recognised. The remanence directions of both polarities are rotated clockwise with respect to the expected directions for mid-Cretaceous/Early Tertiary fields, indicating clockwise rotation of the Candelaria area, including the adjacent batholith, through at least 45° since the acquisition of the normal and reversed remanence components, i.e. since 83 Ma. This case study illustrates the importance of understanding the magnetic behaviour of different ore types, and incorporating self-demagnetization into modelling procedures for highly magnetic targets in mineral exploration.

1. Introduction

Iron oxide copper-gold deposits (IOCGs) contain large amounts of iron oxides, which are extremely dense and, in the case of magnetite-rich deposits, highly magnetic. Forward modelling of magnetic data over magnetite-rich sources, such as IOCGs, is both geologically and geophysically problematic and quantifying the effects of remanence and self-demagnetization is critical. However, measurement of remanence is often neglected and the importance of remanence in IOCGs is poorly understood.

Self-demagnetization is commonly ignored because it is perceived only to affect the intensity of magnetization, and not to have a significant impact on the geometry of the causative body. However, it is well known that self-demagnetization may lead to rotation of the magnetic field vector towards the longest axis of a pipe-like body and towards the plane of a sheet-like body (Clark, 2000; Clark and Emerson, 1999; Clark and Schmidt, 1994; Gay, 1963; Gidley, 1988; Guo et al., 1998,

* Corresponding author at: Mineral Resources Flagship, PO Box 136, North Ryde, NSW, 1670, Australia. Tel.: +61 2 9490 8876; fax: +61 2 9490 8921.
E-mail address: james.austin@csiro.au (J. Austin).
[1] Tel.: +61 2 9490 8876; fax: +61 2 9490 8921.

http://dx.doi.org/10.1016/j.jappgeo.2014.08.002
0926-9851/

2001; Hillan, 2013b; Krahenbuhl and Li, 2007; Zietz and Henderson, 1956). Hence, the self-demagnetisation effect may cause highly magnetic bodies to be mis-modelled

In this study, we review the magnetic properties of IOCG mineralization and present detailed rock property measurements, including magnetic susceptibility and remanent magnetization from the Candelaria deposit, Chile (Fig. 1). The results were used to constrain a simplified magnetic forward model of the deposit. The simplified model is used to quantify the effects of self-demagnetization using new code by Hillan (2013a). Some of the pitfalls associated with determination of magnetic properties, e.g. drilling-induced overprinting, are explored, and the relative importance of remanence and self-demagnetization in magnetite-rich IOCGs is evaluated.

2. Background

2.1. Induced vs remanent magnetization

Magnetism within most rocks containing magnetic minerals will be comprised of two components, induced and remanent magnetization, and it is important to consider both when modelling geological bodies. Induced magnetization is a response to the ambient field and is equal to the product of the magnetic susceptibility and the inducing field. For isotropic rocks, it is parallel to the internal inducing field, which for weakly magnetic rocks is essentially along the regional geomagnetic field direction. Remanent magnetization is a more-or-less permanent magnetization present in the rock, i.e., it is not induced by the present Earth's field, but is retained in the rock over geological time spans by fine-grained particles of minerals such as magnetite, pyrrhotite and hematite. Natural remanent magnetization (NRM) is often acquired during thermal or metasomatic events. As rocks cool through the Curie point they acquire a thermoremanence along the magnetic field direction of the earth at that time. Similarly new magnetic mineral grains forming at temperatures below the Curie point acquire chemical remanent magnetization. The orientation of remanent magnetization can be stable for billions of years, or it can be highly dynamic, acquiring new magnetization over days to years. Its stability is primarily a function of grain size. Magnetite grains larger than about 1 μm form magnetic domains of opposite polarity (Fig. 2A), which reduce the magnetostatic energy of the grain. For magnetite grains larger than 10 μm there are scores of domains within the grain. These grains fall into the large multidomain (MD) size range. In finer grained magnetite (e.g., <0.1 μm) the energy required to form magnetic domain walls is too great, so a single domain structure is retained (Fig. 2B). Not surprisingly, remanence in large MD magnetite is easily changed by exposure to magnetic fields or by thermal fluctuations (even at ambient temperatures), due to movement of domain walls, whereas remanence in single domain magnetite is very stable and intense (Butler, 1992; Dunlop and Özdemir, 1997).

2.2. Typical magnetic properties of IOCGs

Numerous hysteresis and coercivity studies on magnetite-rich IOCGs, such as Starra and Osborne (Clark, 1988), Ernest Henry (Clark, 1994), Candelaria (Clark et al., 2003), Tjårrojåkka (Sandrin and Elming, 2006); the Great Bear magmatic zone (Hayward et al., 2013), Monakoff (Austin et al., 2013a) and Brumby (Austin et al., 2013b) have shown that remanent magnetization present in magnetite-rich IOCGs is primarily carried by MD magnetite, and is unstable (i.e., has a low coercivity). Because the magnetization is so unstable, the measured "natural remanent magnetization" (NRM) in IOCGs is often not "natural" at all, and a large proportion of the total remanent magnetization may be acquired by stress release in the magnetic field within the steel drilling rods. This induces remanent magnetization along the drill hole axis, generally oriented up the hole in the southern hemisphere, and down the hole in the northern hemisphere. This phenomenon may lead workers to overestimate the importance of remanence in IOCGs, as illustrated for the Brumby IOCG in Austin et al. (2013b). "Cleaned" NRM vectors, more representative of in situ NRM, can be obtained by applying low temperature demagnetization, i.e., using liquid nitrogen to cool rocks through the Verwey transition, and rewarming to room temperature, in zero field (e.g., Schmidt, 1993). In general, it is difficult to determine the original in situ magnetization vectors where strong drilling induced overprinting has occurred.

When correctly treated and measured, remanence in magnetite-rich IOCGs is typically subordinate to induced magnetization, although not

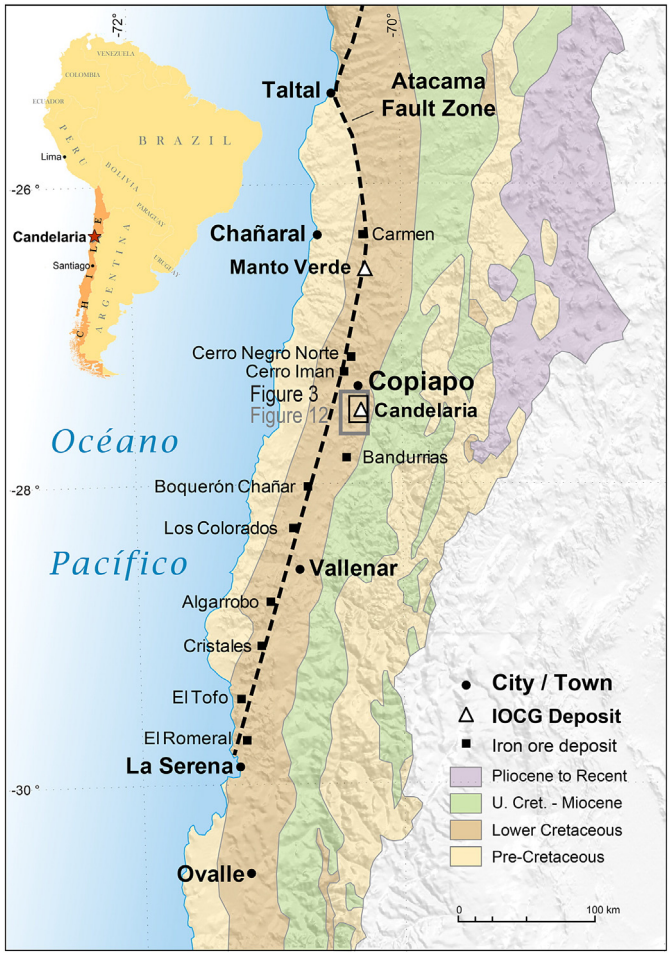

Fig. 1. Simplified geological map of Northern Chile showing the location of major iron and iron oxide copper-gold deposits relative to the Atacama Fault Zone; after Marschik and Fontboté, 2001. Boxes outlining the areas depicted in Figs. 3 and 12 are shown in black and grey respectively.

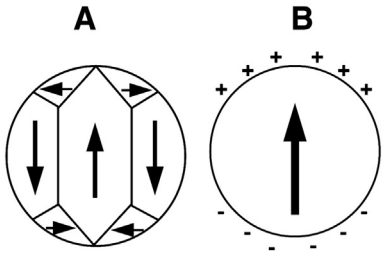

Fig. 2. Shows the difference between multidomain magnetism and single-domain magnetism; A. Grain of ferromagnetic material >10 μm subdivided into domains (multidomain) which reduce the magnetostatic energy of the grain. B. Uniformly magnetized <0.1 μm single-domain grain where magnetization is shown by the arrow, and surface charge by + and − . Grains that are intermediate are called pseudo single domain. (From: Butler, 1992.)

completely negligible. For example, IOCGs of the Cloncurry District commonly have high magnetic susceptibilities (e.g., 0.7–2 SI) but remanence commonly accounts for <20% of induced magnetization (e.g., Austin et al., 2013a,b; Clark, 1988, 1994; Clark et al., 2003). The ratio between remanent and induced magnetization (called the Koenigsberger ratio, Q) is therefore <0.2. Specimens of IOCG ore sampled directly from the pit of the Monakoff, where one can be confident that the samples are not overprinted by drilling or lightning induced IRM, have a mean Q of 0.16 (Austin et al., 2013a), and of the total remanent magnetization, approximately 70% is held in low coercivity (magnetically "soft") MD magnetite (Austin et al., 2013c). Furthermore, the NRM carriers are large MD magnetite grains, and the remanent magnetization is dominantly viscous and oriented parallel to the inducing field, so the effect of the remanence is simply to augment the induced component by 10–20%. Pyrrhotite, which is found in very high concentrations in parts of the Brumby IOCG prospect (Austin et al., 2013b), can have extremely high Koenigsberger ratios (e.g., >100) corresponding with significant susceptibility (e.g., 0.3 SI). However, the limited volume of pyrrhotite within most IOCGs does not contribute significantly to their total magnetic anomalies. Although remanence is commonly not significant in IOCGs it can be for other styles of mineralisation, e.g., magmatic nickel sulphide deposits (e.g., Austin et al., 2014), skarns (e.g., Clark and Lackie, 2003), porphyries (e.g., Astudillo et al., 2010; Clark, 2014), and strata-bound copper (e.g., Townley et al., 2007).

3. Geology of the Candelaria IOCG

The regional stratigraphy, structures, mineralogy, paragenesis, and alteration observed at Candelaria are discussed in detail by Marschik and Fontboté (2001), as summarised below.

The Candelaria iron oxide copper-gold (IOCG) deposit sits east of branches of the Atacama Fault Zone (Fig. 1), which stretches >1000 km along the Chilean coast. The fault zone is a strike-slip system, related to subduction in the west, which originated during the Jurassic (Dallmeyer et al., 1996; Marschik and Fontboté, 2001; Scheuber et al., 1995). It is thought to control the localization of iron deposits in the Chilean iron belt (e.g., Bookstrom, 1977; Espinoza, 1990; Thiele and Pincheira, 1987) within the coastal cordillera.

The Candelaria-Punta del Cobre IOCGs are hosted in the Early Cretaceous Punta del Cobre Formation (Fig. 3), which consists of subduction related volcanics and volcaniclastics sitting adjacent to the Chilean coastal batholith (Marschik and Fontboté, 2001). Facies are transitional from continental volcanic arc lithologies in the west to shallow marine lithologies in the east (Chañarcillo Group; Marschik and Fontboté, 2001). Deposition of the upper volcanic–volcaniclastic unit (Punta del Cobre Formation) commenced in the Berriasian (Early Cretaceous), followed by deposition of 1700–2000 m of carbonates (Chañarcillo Group) during the Valanginian to Aptian (Marschik and Fontboté, 2001). Basin inversion and subsequent partial erosion of the back-arc sequence commenced in the late Aptian at ca 115 Ma (Jurgan, 1977; Segerstrom and Parker, 1959; Zentilli, 1974) and the Copiapó batholith intruded at ca 110 Ma (Arévalo, 1999), causing an extensive contact metamorphic aureole in the district (Tilling, 1962, 1963, 1976). The Candelaria deposit contains altered dacitic dikes and sills that locally contain minor sulfide mineralization and parts of the batholith are affected by intense sodic(-calcic) alteration related to mineralization (Marschik and Fontboté, 2001).

The Candelaria mine sits within a large northeast-plunging antiform (the Tierra Amarilla anticlinorium; Marschik and Fontboté, 2001), which is displaced by a southeast-verging fold-thrust system (El Bronce fold-thrust system; Arévalo and Grocott, 1997; Marschik and Fontboté, 2001), and cut by a large number of NNW- to NW-oriented sinistral strike-slip faults. The strike-slip faults represent the main structural control on mineralization at Candelaria (Camus, 1980; Marschik and Fontboté, 1996, 2001). Numerous reverse and strike-slip ductile shear zones (e.g., Ojancos and Candelaria-Florida shear Zones) which formed between the Berriasian and Aptian, predate copper mineralization at Candelaria (Marschik and Fontboté, 2001). They are cut by sinistral NNW–NW oriented strike-slip faults, ENE-oriented strike-slip faults, and by NE-oriented moderately west dipping faults (Marschik and Fontboté, 2001).

The Candelaria orebody (Fig. 4) is in general composed of magnetite with minor hematite, chalcopyrite and pyrite, and locally contains

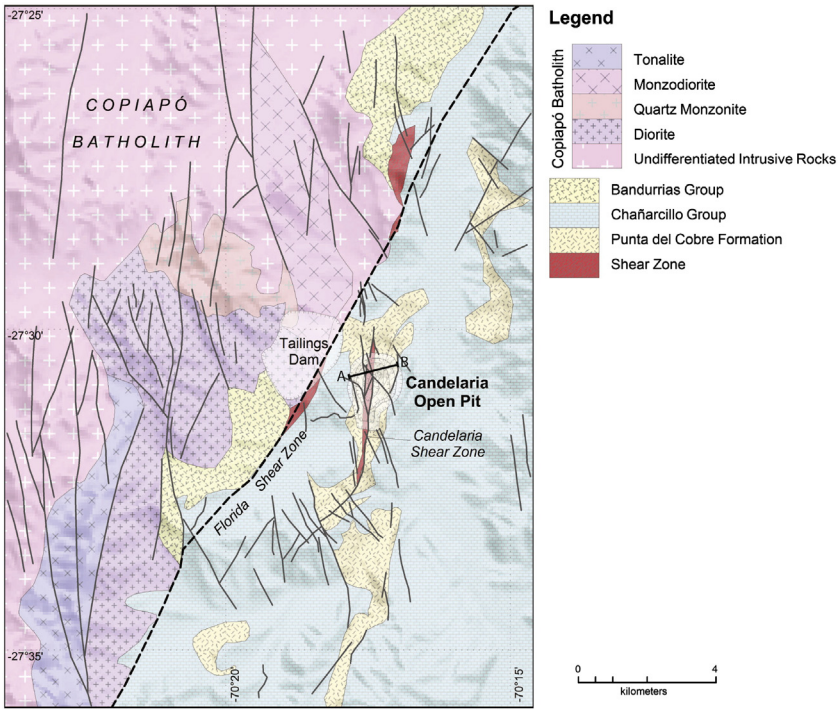

Fig. 3. Simplified geological map of the area surrounding the Candelaria Cu–Au deposit. The NNE-trending Florida shear zone is a splay off the Atacama Fault Zone. This and the north-trending Candelaria Shear Zone predate the north to north-northwest trending faults. Modified from Marschik and Fontboté (2001).

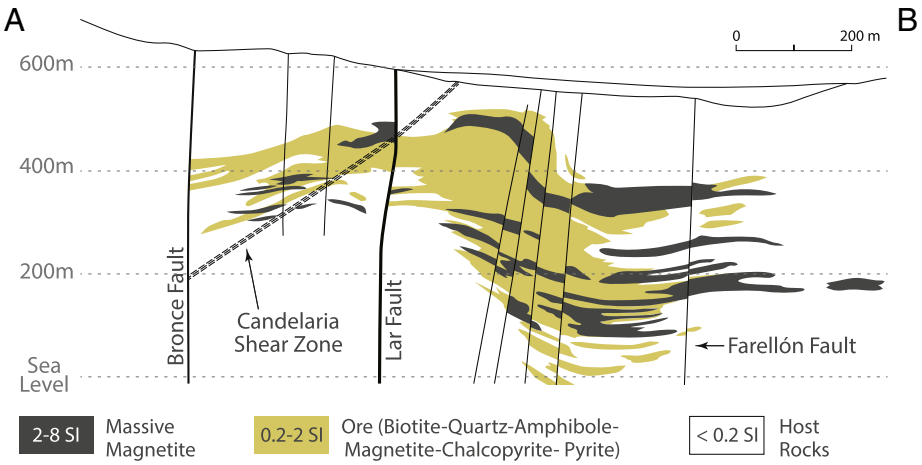

Fig. 4. Simplified geological cross-section of the Candelaria deposit as marked by the line A–B on Fig. 3. In this version of the cross-section we show the geology in terms of its magnetic properties. Massive magnetite which is highly magnetic, ranging from approximately 2 to 8 SI, Cu–Au ore which is of moderate to high magnetic susceptibility, and host rocks which are relatively non-magnetic. Modified from Marschik and Fontboté (2001).

pyrrhotite, sphalerite, and trace quantities of molybdenite and arsenopyrite (Marschik and Fontboté, 2001). Gold sits within microscopic inclusions in chalcopyrite, within microfractures in pyrite (Ryan et al., 1995) and in an Hg–Au–Ag alloy (Hopf, 1990). At Candelaria, copper is hosted in veins, the matrix of breccias, but more importantly overprints massive magnetite replacement bodies (i.e., mantos; Fig. 4) and replaces pore space, forming bodies that are approximately concordant with stratification. Gangue minerals commonly include quartz and anhydrite (Marschik and Fontboté, 2001), while tourmaline and trace fluorite occur locally (Hopf, 1990). Candelaria, contains <0.1% light rare earth elements (Marschik et al., 2000). Supergene enrichment zones include malachite, chrysocolla, chalcocite, and covellite (Sillitoe and Clark, 1969). Large orebodies in the district, such as Candelaria, often occur at the intersection of NW- to NNW-oriented faults with the Geraldo-Negro and Algarrobos members' contact and are spatially coincident with biotite–quartz–magnetite, plus sodic and/or potassic alteration (Marschik and Fontboté, 2001).

The paragenetic sequence at Candelaria (summarized in Fig. 5) comprises intense iron metasomatism, associated with early potassic alteration and silicification, which post-dated large-scale early pervasive albitisation (Marschik and Fontboté, 2001). Both Ti-rich, brown (TiO_2 > 2.0 wt.%) and green hydrothermal biotite (TiO_2 < 1.8 wt.%) are associated with widespread pervasive magnetite alteration. Iron metasomatism resulted in precipitation of specular hematite, mainly in fractures, and temporally equivalent massive magnetite replacement. These were overprinted by specularite, mushketovite and the generation of new magnetite due to an increasingly reducing environment and/or higher temperatures. The majority of copper mineralization, which post-dates early Fe-oxide precipitation, comprises chalcopyrite ± pyrite crosscutting magnetite or specularite (Marschik and Fontboté, 2001). Arévalo et al. (2006) presented microstructural and geochronological evidence showing that the main mineralization stage was coeval with the San Gregorio plutonic complex and movement on the Ojancos-La Florida shear zone.

4. Magnetic properties of Candelaria IOCG

4.1. Sampling

Sun-oriented blocks were collected from exposures in the north pit of the Candelaria mine. Three localities represent the magnetite and/or hematite-rich mineralisation within the Lower Andesite unit, and the other two represent skarns located within the Upper Andesites. Diorite samples belonging to the Mid-Cretaceous batholith were collected at two sites.

In addition, representative samples of oriented drill cores from holes SO-009, SO-010 and SO-011 were taken. Each sample was re-drilled to

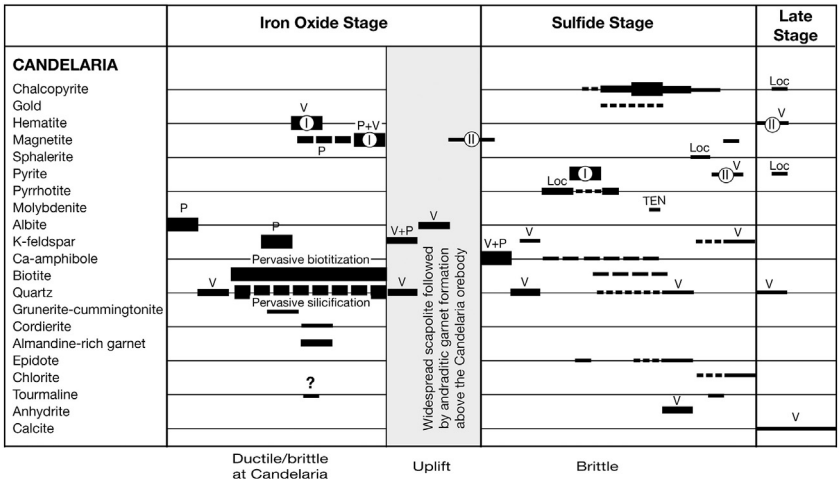

Fig. 5. Alteration paragenesis, modified from Marschik and Fontboté (2001). The observed overprinting relationships are similar to those observed for a variety of IOCGs in the Cloncurry District, Qld, Australia. Abbreviations are after Marschik and Fontboté (2001): P = pervasive alteration, TEN = tentatively, V = veinlets, ? = uncertain.

obtain cylindrical specimens of 2.5 cm diameter and 2.2 cm height, for palaeomagnetic measurements.

4.2. Methods and techniques

Standard palaeomagnetic procedures were followed to determine the basic magnetic properties. A CSIRO susceptibility bridge (Ridley and Brown, 1980) was used to measure absolute magnetic susceptibility. The true susceptibilities along the axis of the specimens were calculated by correcting for the self-demagnetization effect on apparent susceptibility of strongly magnetic specimens, following the procedure described by Schmidt and Clark (1994).

The natural remanent magnetisation (NRM) was measured either with a 2G cryogenic magnetometer or with a DIGICO spinner magnetometer, and corrected for the self-demagnetization effect. NRM that is more representative of the in situ remanence carried by multidomain magnetite-bearing rocks was obtained after applying low temperature demagnetisation using liquid nitrogen. This palaeomagnetic cleaning technique largely removes the contamination induced by drilling, exposure to pencil magnets, or other causes which often affect the remanence of MD magnetite. The combined NRM (J) for each sample is calculated as the vector sum of the individual specimen NRMs, divided by the number of specimens.

The Koenigsberger ratio (Q) was calculated as J/kF, where k is the susceptibility and F is the geomagnetic field strength in equivalent units to J (B = 22,300 nT, F = 17,750 mA/m). The stability of the NRM was evaluated by applying complete demagnetization procedures to selected specimens from every site. Alternating field (AF) demagnetization was carried out by means of the static demagnetizer attached to the 2G magnetometer. Stepwise thermal demagnetization was performed with the CSIRO programmable carousel furnace. Linearity spectrum analysis (LSA, Schmidt, 1982) was used to identify linear segments for groups of specimens from the same site or drill core. Hysteresis loops were determined in representative samples by means of a variable field translation balance (VFTB).

5. Results

Bulk susceptibilities, remanence vectors and Koenigsberger ratios are presented in Table 1. Most of the samples have high bulk susceptibilities due to the presence of magnetite. The highest values (2–8 SI) were observed in semi-massive magnetite sampled in pit exposures and in hole SO-011. Scattering of the NRM directions is higher for the most magnetic samples, and can be attributed to spurious components. In contrast, the "cleaned" remanence directions were less scattered and more representative of the undisturbed in situ NRM directions. Alternating field (AF) cleaning in a 10 mT field removed most sources of palaeomagnetic noise in these samples.

Despite magnetic cleaning, NRM directions of the ore samples are scattered, as strongly magnetic samples contain abundant multidomain magnetite that is not capable of carrying a very stable remanence, and because remanence was acquired in a highly magnetic environment which produced strong local deflections of the magnetic field. Most NRM directions plot broadly in the NE quadrant of a stereonet, with moderate negative (upward) inclination; some samples, however, have positive (downward) inclination (Fig. 6A). Samples taken in the Copiapó Batholith and the skarn assemblages were less magnetic and therefore more clustered, revealing a dominant group in the NE up octant and a subordinate, antipodal, cluster in the SW down octant (Fig. 6B).

Table 1
Magnetic properties of Candelaria samples.

Site/	Rock unit	Alteration	Mineralisation	N	Susceptibility	NRM			Q
Sample					(10–3 SI)	Dec	Inc	J (A/m)	
can01	Lower andesite	Bio-qtz-amph-mt-cp (py, hm)	Mt-manto	24	4949.0	249.2	−29.6	18.192	0.25
can02	Lower andesite	Bio-qtz-amph-mt-cp (py, hm)	orebody	17	2597.7	11.9	−60.8	5.809	0.18
can03	Lower andesite	Bio-qtz-amph-mt-cp (py, hm)	Mt-manto	14	8153.5	49.6	−36.4	30.699	0.32
can04	Upper andesite	Bio ovp by pyx-scap (skarn)	Host rock	23	0.3	37.6	−34.8	0.005	1.20
can05	Upper andesite	Bio ovp by pyx-scap (skarn) + mt	Host rock	13	87.5	345.4	−36.0	0.424	0.51
can06	Diorite	–	Diorite	16	35.3	51.7	−45.8	0.557	0.65
can07	Diorite	–	Diorite	4	39.4	48.3	−41.5	0.169	0.28
09–077 m	Upper andesite	Bio ovp by pyx-scap (skarn)	Host rock	5	1.9	11.7	−24.7	0.019	0.58
09–135 m	Upper andesite	Bio ovp by pyx-scap (skarn)	Host rock	4	1.8	249.3	−5.7	0.001	0.02
09–142 m	Upper andesite	Bio ovp by pyx-scap (skarn)	Host rock	5	1.2	52.2	−23.5	0.001	0.06
09–171 m	Dacite sill	Pyx-scap + mt	Host rock	5	702.3	333.8	−66.9	10.250	0.91
09–180 m	Dacite sill	Pyx-scap ovp by Kfdsp	Host rock	4	59.0	174.8	74.7	0.255	0.25
09–205 m	Upper andesite	Bio ovp by pyx-scap (skarn) + mt	Host rock	5	389.7	56.9	−10.5	1.542	0.25
09–214 m	Upper andesite	Pyx-scap-(Kfsp-amph-chl-ep)	Host rock	6	70.2	24.3	−53.5	0.246	0.21
10–051 m	Upper andesite	Bio-plg	Host rock	4	96.6	4.2	2.6	0.629	0.39
10–061 m	Upper andesite	Bio-plg	Host rock	5	59.8	43.0	−19.0	0.036	0.04
10–073 m	Upper andesite	Bio-plg-qtz	Host rock	5	1.0	183.2	1.3	0.008	0.46
10–250 m	Tuff	Gar-bio	Host rock	4	0.9	113.4	−14.6	0.002	0.10
10–279 m	Tuff	Bio-plag-(Kfsp-qtz-mt-mt)	Host rock	5	125.7	142.6	50.6	0.351	0.20
10–296 m	Lower andesite	Mt breccia (pyx-scap-mt-(chl-amph-cp-py))	Orebody	6	184.9	68.6	−28.1	0.935	0.34
10–297 m	Tuff	Pyx-scap-(cp, py, po)	Host rock	5	62.0	109.2	−18.8	0.091	0.13
10–298 m	Tuff	Pyx-scap	Host rock	4	224.6	77.8	41.8	0.231	0.17
10–308 m	Tuff	Amph-Kfsp-chl-sph-scap-(mt, cp, py)	Host rock	4	46.3	12.2	−64.5	0.044	0.09
10–315 m	Lower andesite	Bio-qtz-(mt, cp, py)	Host rock	6	116.4	241.7	−78.6	0.151	0.11
10–322 m	Lower andesite	Bio-qtz-(mt, cp, py)	Host rock	4	2.9	250.8	25.3	0.079	1.52
11–275 m	Lower andesite	Bio-plag-(qtz, mt, amph)	Host rock	5	47.7	47.6	−26.2	0.215	0.29
11–303 m	Lower andesite	Mt breccia (bio-pyx-scap-mt-cp-(py))	Orebody	5	2275.4	221.8	44.7	10.623	0.28
11–311 m	Lower andesite	Mt breccia (bio-pyx-scap-mt-cp-(py))	Orebody	5	2054.8	55.6	−25.5	12.556	0.39
11–322 m	Lower andesite	Bio-plag-qtz-(mt-amph)	Host rock	6	343.4	55.8	−43.4	1.955	0.35
11–333 m	Lower andesite	Bio-plag-qtz-(mt-amph)	Host rock	6	258.6	65.0	−47.7	1.225	0.28
11–338 m	Lower andesite	Bio-plag-qtz-(mt-amph)	Host rock	3	156.4	315.9	72.0	0.049	0.02
Orebody					3369.21	34.3	−60.6	5.860	0.10
Host rocks					124.18	16.1	−60.1	0.600	0.27
Diorite					37.37	50.9	−44.8	0.363	0.55

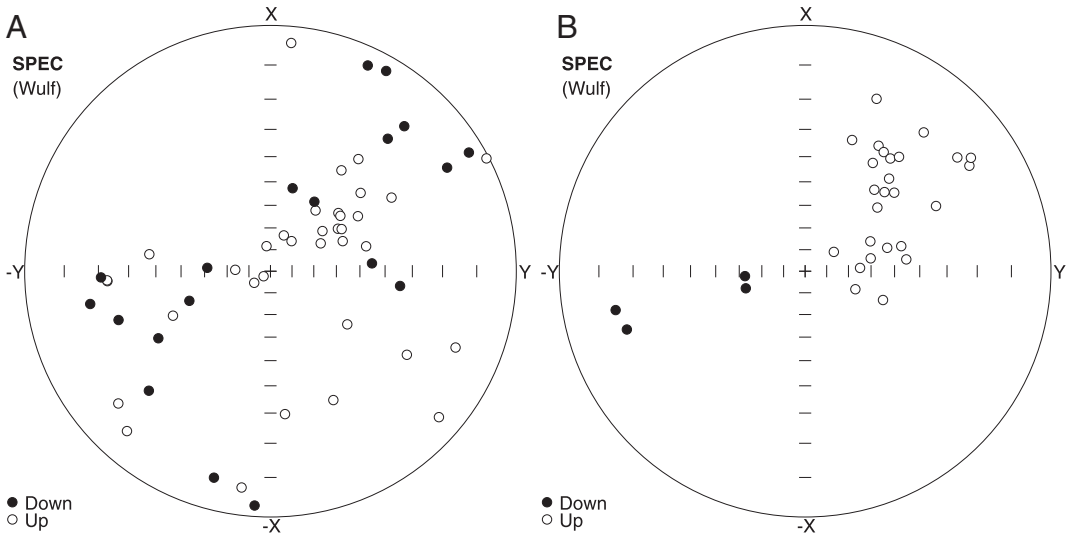

Fig. 6. Stereograms of "cleaned" remanence directions (10 mT AF) from A) the Candelaria orebody, and B) the batholith and skarn samples. Open symbols are on the upper hemisphere (negative inclinations), and filled symbols are on the lower hemisphere (positive inclinations).

The Koenigsberger ratios (Q) of the samples are typically much less than one, indicating that remanence is subordinate to induced magnetisation for these samples. This conclusion is reinforced by the partial cancellation of remanent magnetisations within the orebody due to the presence of opposite polarities. The direct implication of this, i.e., that magnetic anomalies in the area should be controlled by induced instead of remanent magnetisation, is at odds with previous proposed models (Taylor, 2000) as will be discussed later.

5.1. Stability of remanence

A substantial part of the remanence of the ore samples (60–80%) was removed by low temperature demagnetisation, as shown in Fig. 7, which indicates that multidomain magnetite is the main carrier of the NRM. Alternating frequency (AF) demagnetisation almost completely removes the remanence of strongly magnetic rocks in applied peak fields of 30–50 mT (Fig. 7A). Thermal demagnetisation produced noisy results; however, remanence was erased with temperatures of 550–580 °C (Fig. 7B), indicating that the remanence is carried almost exclusively in magnetite (and or mushketovite).

Detailed analysis of remanence components isolated by AF and thermal demagnetisation revealed a complex history of overprinting in these rocks and ores. Fig. 7 shows that the remanence of a semi-massive magnetite ore sample from site 2 in the pit is dominated by a NE up (normal) component of moderate coercivity that is removed steadily up to 50 mT, whereas another ore sample from site 3 shows only a reversed component that is stable to ~570 °C (Fig. 7C and D).

This behaviour characterizes all the orebody samples and most of the remaining highly magnetic specimens. Results of rock magnetic studies (coercivity and hysteresis) determined that the ore samples tested plotted in the multidomain field on a Day plot (Fig. 8).

Some samples from the Lower Andesite unit are moderately magnetic and show very stable behavior (Fig. 9). The sigmoid shape of the AF demagnetisation curve (Fig. 9A) and the discrete unblocking temperature at ~570 °C (Fig. 9C) indicate the presence of single domain magnetite, which is submicron in size. An intermediate behaviour between the two described above was observed in a few sites, suggesting

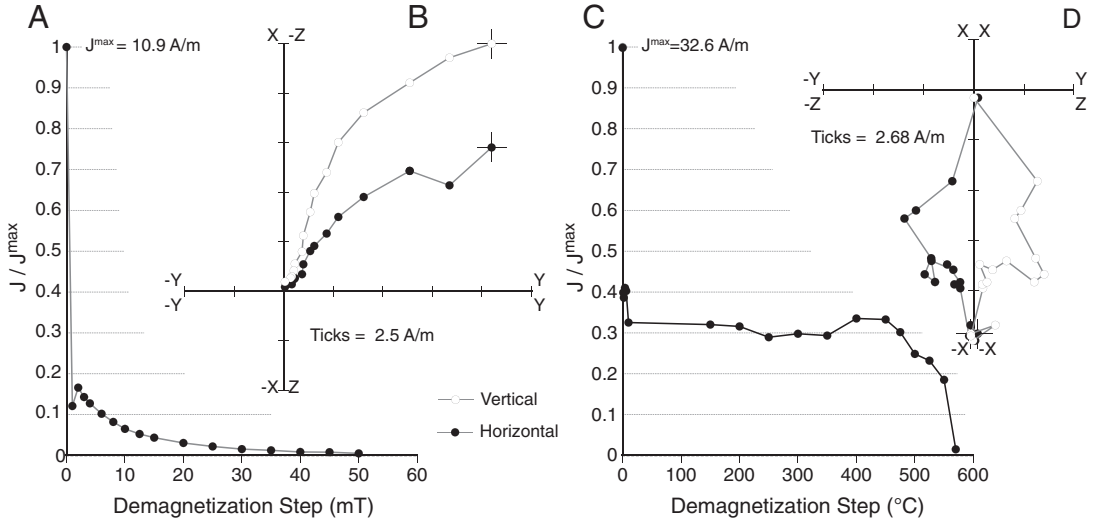

Fig. 7. Demagnetisation behavior of ore rocks: A, B) AF demagnetisation (Can02-B3) shows only a NE up (normal) component of moderate coercivity; C, D) Thermal demagnetisation of Can03-A2 shows only a reversed component that is stable to ~570 °C. a) and c) are plots of magnetisation intensity vs. demagnetisation step; b) and d) are Zijderveld plots. Note that approximately 50–80% of remanent magnetization is removed by application of low temperature demagnetization (LN), and the samples are almost completely demagnetized in a field of 50 mT or after heating to 550–570 °C.

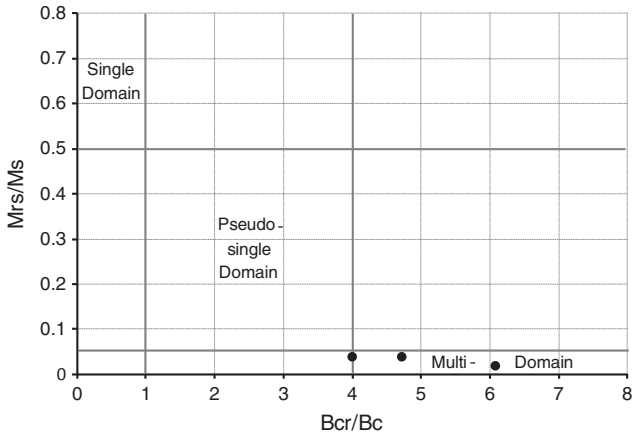

Fig. 8. A Day plot (Day et al., 1977) correlating Mrs/Ms (Saturation Remanent Magnetization/ Saturation Magnetization) and Bcr/Bc (Coercivity of Remanence/ Rock Coercivity) to identify magnetic domain structure. The results for specimen 10-296, CAN02A and CAN03B all plot in the multi-domain field, indicating that their magnetisation is relatively unstable.

the presence of pseudo-single domain magnetite grains in the size range of 1–20 μm.

Weakly magnetic skarn specimens have a very stable, single, NE up component, which could not be removed with peak fields as high as 100 mT, but was unblocked with temperatures of 300–350 °C (Fig. 10). Judging from its demagnetisation characteristics and the NRM intensity (Fig. 10), it can be concluded that the remanence is probably carried by trace amounts of fine-grained monoclinic pyrrhotite.

Samples from dioritic rocks of the batholith carry remanence with moderate to high stability to AF (Fig. 11), which thermal demagnetisation unblocks predominantly between 500 °C and 580 °C, indicating that the main magnetic carrier is pseudosingle-domain magnetite. Fig. 11A,B illustrates a diorite sample that carries a single normal polarity component of high coercivity, stable to 100 mT. However, in a similar sample, AF demagnetisation revealed a subordinate reversed component that was removed in fields between 2 mT and 20 mT, superimposed on the NE up component that is stable up to 100 mT (Fig. 11B). Thus even the batholith records a subtle overprinting event with reversed polarity. The stable normal polarity remanence is interpreted as primary, dating from initial cooling of the mid-Cretaceous diorite intrusion.

5.2. Palaeomagnetic directions

The main intrusive and hydrothermal events in the Candelaria area are mid-Cretaceous in age, and therefore they occurred during the Cretaceous normal polarity superchron, which lasted from 118 Ma to 83 Ma. Thus remanence directions recorded at Candelaria are expected to be of normal polarity. Fig. 6 shows that remanence directions from the magnetite-rich orebody are somewhat scattered, even after AF cleaning to 10 mT. This may reflect local deflections of the geomagnetic field within the highly magnetic orebody, similar to the deflections of compass needles observed within the Candelaria pit and in bore holes. However, there is a NE dominant grouping with a subordinate SW cluster still apparent in the stereogram (Fig. 6A).

Skarn samples from the pit, within the Upper Andesites, all exhibit normal polarity cleaned directions, as do samples from the batholith; a few skarn samples in hole SO09 show reversed polarity, overall defining relatively well-grouped populations which are antipodal (Fig. 6B). Characteristic remanence directions isolated after complete demagnetisation procedures repeat the pattern observed for 10 mT-cleaned remanence (Fig. 12). The cleaned remanence directions are not exclusively of normal polarity as expected according to the age of hydrothermalism/intrusion, but include reversed components that may be subordinate to the normal component (Fig. 11b), but can completely overprint some samples (e.g., Fig. 7B, 9A).

The skarns and hornfelses that enclose the Candelaria orebody also show clear evidence of a post 83 Ma overprint magnetisation with reverse polarity, although the dominant component is a normal polarity remanence of moderate to high stability which is interpreted as acquired during the alteration event(s) that precipitated the magnetic minerals (predominantly magnetite). The presence of the reversed polarity overprint suggests that the Candelaria deposit and its immediate environs have experienced a post 83 Ma thermal or thermochemical event that has not been previously reported in published geochronological studies.

The remanence directions of both polarities are rotated clockwise with respect to the expected directions for mid-Cretaceous/Early Tertiary fields, which for an unrotated terrane at this latitude are north (3°) with moderate negative inclination (normal polarity) or south with moderate positive inclination (reverse polarity). A comparison in VGP (virtual geomagnetic pole) space can be attempted by the method of Beck et al. (1986), between the pole calculated from the stable remanence carried by the diorite, for instance, and the Aptian reference pole for South America given by Geuna et al. (2000). This gives a clockwise

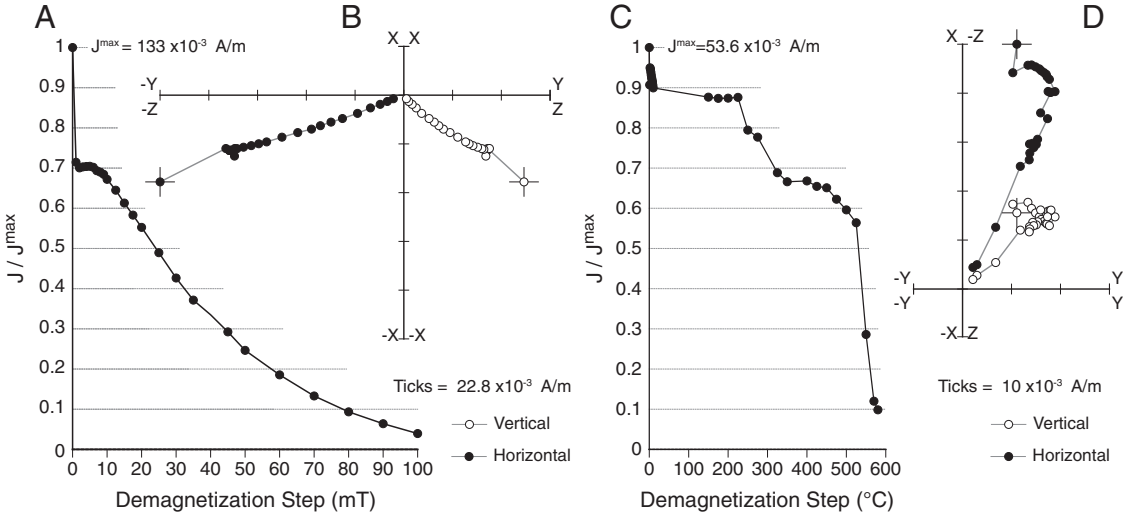

Fig. 9. Demagnetisation behavior of contact metamorphosed andesite specimens: a, b) AF demagnetisation (SO10-322a); c, d) thermal demagnetisation (SO09-077a). a) and c) are plots of magnetisation intensity vs. demagnetisation step; b) and d) are Zijderveld plots. Stable remanent magnetization is 50% stronger than induced magnetization (i.e. Q = 1.5, see Table 1).

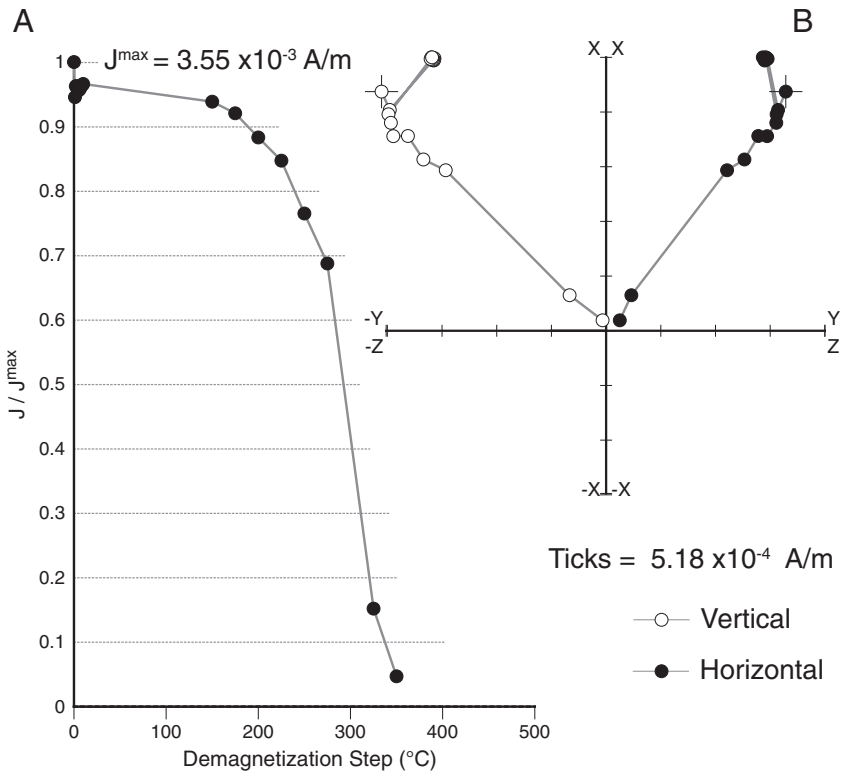

Fig. 10. A combination of AF and thermal demagnetisation carried out on a skarn specimen from site 4, Can04A1, displaying demagnetisation at ~350 °C, and very stable remanence under AF-demagnetisation. A) Shows a plot of magnetisation intensity (y) vs demagnetization step (x) in°C; B) shows the southwest quadrant of a Zijderveld plot of demagnetization.

rotation of 48.4 ± 9.6 with minimum poleward apparent translation (*P* 0.9 ± 8.6). This indicates clockwise rotation of the Candelaria area, including the adjacent batholith, through at least 45° since the acquisition of the normal and reversed remanence components, i.e. since 83 Ma. The sense and magnitude of rotation is consistent with substantial clockwise rotations reported from paleomagnetic studies of northern Chile between 25°S and 27°S (e.g., Arriagada et al., 2000, 2003; Taylor, 2000). This rotation appears to be unrelated to the dominant sinistral transpression observed in the area (e.g., Arévalo et al., 2006), which would have caused counter-clockwise rotation. Taylor (2000) suggested that the rotation was caused by large scale folding related to the Arica defection/ Bolivian Orocline. However, Arriagada et al. (2003) found that the majority of the rotation occurred during the Eocene–early Oligocene Incaic Orogeny, and hence, that the development of the Bolivian orocline during late Neogene could not be explained by simple bending of the entire margin.

6. Modelling the magnetic properties of IOCGS

Although remanence is relatively easily measured, some authors infer that remanence is dominant in IOCG deposits based only on interpretation of the magnetic field data. For example, Ellis et al. (2012) used

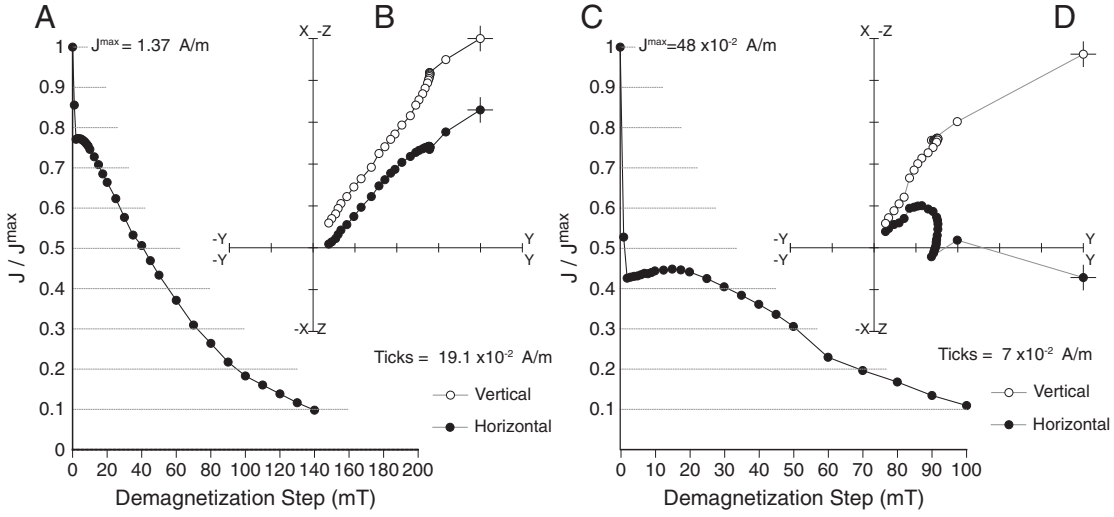

Fig. 11. AF demagnetisation behavior of diorite samples (Copiapó Batholith): A, B) Can06-B2, displaying stable NE-directed magnetization up to at least 140 mT; C, D) Can06-A2, displaying a subordinate reversed component, removed in fields between 2 mT and 20 mT, superimposed stable NE-directed magnetization up to at least 140 mT. A) and C) are plots of magnetisation intensity vs. demagnetisation step; B) and D) are Zijderveld plots.

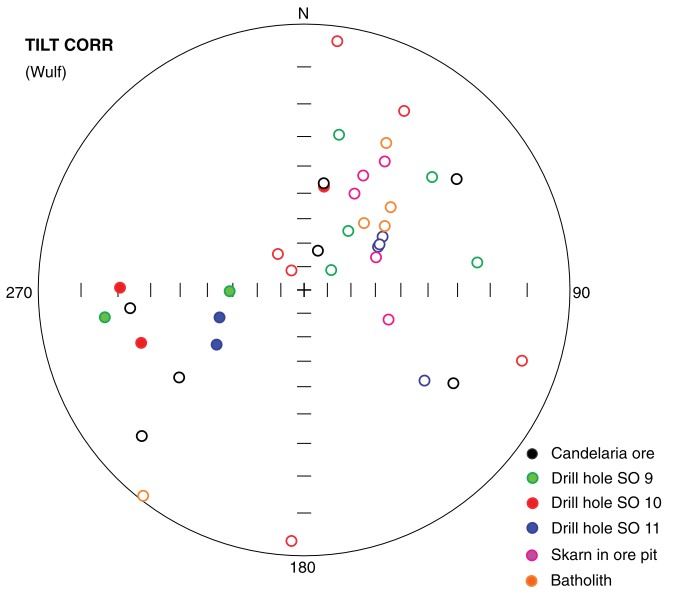

Fig. 12. Stereograms of "cleaned" remanence directions obtained after complete AF and/or thermal demagnetisation of pilot specimens (two per site) from the Candelaria orebody, drill hole SO9, hole SO10, hole SO11, skarn samples from the Candelaria pit and the Copiapó Batholith. Open symbols are on the upper hemisphere (negative inclinations), and filled symbols are on the lower hemisphere (positive inclinations).

a 3-D voxel-based inversion to derive total magnetization vectors, from which they infer remanence to be significant at Osborne. However, their inference conflicts with measured data (Clark, 1988) which demonstrates that remanence is minor and that the modelling difficulties at Osborne are due to self-demagnetization and, to a lesser extent, distortion of the regional geomagnetic field direction by the intense magnetic anomaly associated with the Osborne deposit (Clark, 2000; Gidley, 1988). Similarly, Taylor (2000) suggested that the complexity of Candelaria's magnetic anomaly was caused by remanence. The magnetic anomaly over the Candelaria deposit displays a distinct pattern of NNE–SSW aligned W to WNW-striking anomalies that are repeated to the NNE and SSW along a splay off the Atacama Fault Zone (Fig. 13).

Taylor (2000) took the existence of these magnetic lows to both the NNE and SSW of the magnetic highs to be indicative of a strong reverse polarity remanent component, and thus modelled Candelaria using a susceptibility of 0.005 cgs (0.063 SI) and a Koenigsberger ratio of ~5. The remanence is "assumed" to have a declination of 215° and inclination of 40°. Due to some uncertainties relating to the results reported by Taylor (2000), the modelling result was reproduced using Modelvision™ (Fig. 14) and seems an adequate fit to the data (~15% rms error). However, it must be noted that in order to achieve this result the background (regional) field had to be set very high, and thus the low in the southwest is very poorly modelled. Furthermore, the body appears to only occupy the northernmost part of the Candelaria pit. Examination of the regional data shows that Candelaria sits within a highly magnetic environment with strong local gradients, and that neighbouring anomalies strongly interfere with the anomaly. The strongly magnetic environment must be taken into account in any quantitative modelling, because magnetic anomalies arise from magnetization contrasts, not just the absolute magnetization of the assumed causative body.

Analyses presented here show that the Candelaria ore has an extremely high susceptibility of ~3.4 SI, and very weak remanence, which itself is dominated by recent viscous overprinting, aligned parallel to the Earth's Field (as suggested by Roperch et al., 2001). Thus there is no evidence from our collection of samples for the intense reversed remanence inferred for the Candelaria orebody by Taylor (2000), based on modelling of a portion of the associated magnetic anomaly. Furthermore, because the ore is so highly susceptible it will suffer from self-demagnetization effects. Where there is significant remanent magnetisation it would be appropriate to incorporate both remanence and magnetic susceptibility (i.e., an effective medium approximation) to determine a bulk magnetisation intensity and inclination of a given body (e.g., Austin and Foss, 2014). However in this case, the susceptibility of the ore is so strong and the remanence so weak, that we feel justified in simply using the mean value for of the lithologies sampled.

The resultant model (Fig. 15) consists of a number of sub-parallel tabular bodies with extreme (3–4 SI) susceptibility, that dip shallowly (~5°) to the south, and step up to the west, indicating transpressional displacement of the lenses, west over east. The host rocks, which are approximately 30 times less magnetic than the ore, are not incorporated into the model, but are compensated for using the background field. The model uses an estimate of self-demagnetization (built into ModelVision™ software) to compensate for the self demagnetisation effect. The model, is a significant simplification of the geology, but does fit the data well (3.2% rms error) and accounts for the repeating pattern of this style of anomaly at this locality. The Cu–Au mineralisation is spatially adjacent to the highly magnetised "mantos" (sub-horizontal magnetite sheets), but does not contribute significantly to the anomaly due to its significantly lower magnetic susceptibility. Instead we suggest that the Cu–Au mineralisation is related to partial replacement of the highly magnetic mantos along a series of steep, north to NNW-trending faults.

7. Modelling self-demagnetization

Self-demagnetization is an effect present in all magnetic bodies (with non-zero susceptibility) in which the internal fields perturb the ambient field and produce a magnetization different to that expected for a normal induced component. This may be incorrectly interpreted as the influence of a remanent magnetization component. The self-demagnetization effect depends heavily on the shape of the body and its susceptibility. The effects can effectively be ignored for susceptibilities below 0.1 SI, but above this threshold, the demagnetizing fields begin to have a considerable suppression effect on the magnetization, and hence the observed external fields. The magnetization vector is preferentially suppressed along the shorter dimensions of the body and this leads to a rotation of the vector towards the elongate dimensions. The rotation will be more pronounced the greater the elongation, and attains its maximum value for intermediate angles (approximately 45°–75°, depending on the shape and susceptibility) between this direction and the local geomagnetic field. Interactions will also take place between highly magnetic bodies that are nearby, adding further complexity to modelling efforts (Hillan, 2013a).

From the above, it is immediately obvious that the Candelaria model (Fig. 15) of multiple, highly susceptible (3–4 SI), elongate sheets is one that is likely to suffer strongly from self-demagnetization and multiple body interaction effects. As an example, consider a typical sheet representative of the Candelaria model with susceptibility of 3.5 SI and a dimension ratio of 10:17:1 (X:Y:Z). The sheets are dipping shallowly to the south (around 5°) with an east-west strike (rotated around 079° from north), in a local field of approximately 0° declination and −25° inclination. Using the average demagnetising factors for this prism (Aharoni, 1998) we calculate the magnetization direction corrected for self-demagnetization effects to be −8° inclination, 10° declination, and the magnetization intensity to be suppressed by a ratio of approximately 0.77. This is a substantial deviation from a normal isotropically induced magnetization that is proportional to intrinsic susceptibility; therefore, self-demagnetization corrections should be implemented.

The average demagnetization factor for a prism becomes an increasingly erroneous model in the limit of high susceptibilities and for observations close to the discontinuous edges (Hillan, 2013c). Furthermore, there are multiple bodies to consider in the case of the Candelaria model developed above. A more accurate forward model may be computed using the point varying demagnetization tensor, here implemented in the Fourier domain for speed (Beleggia and De

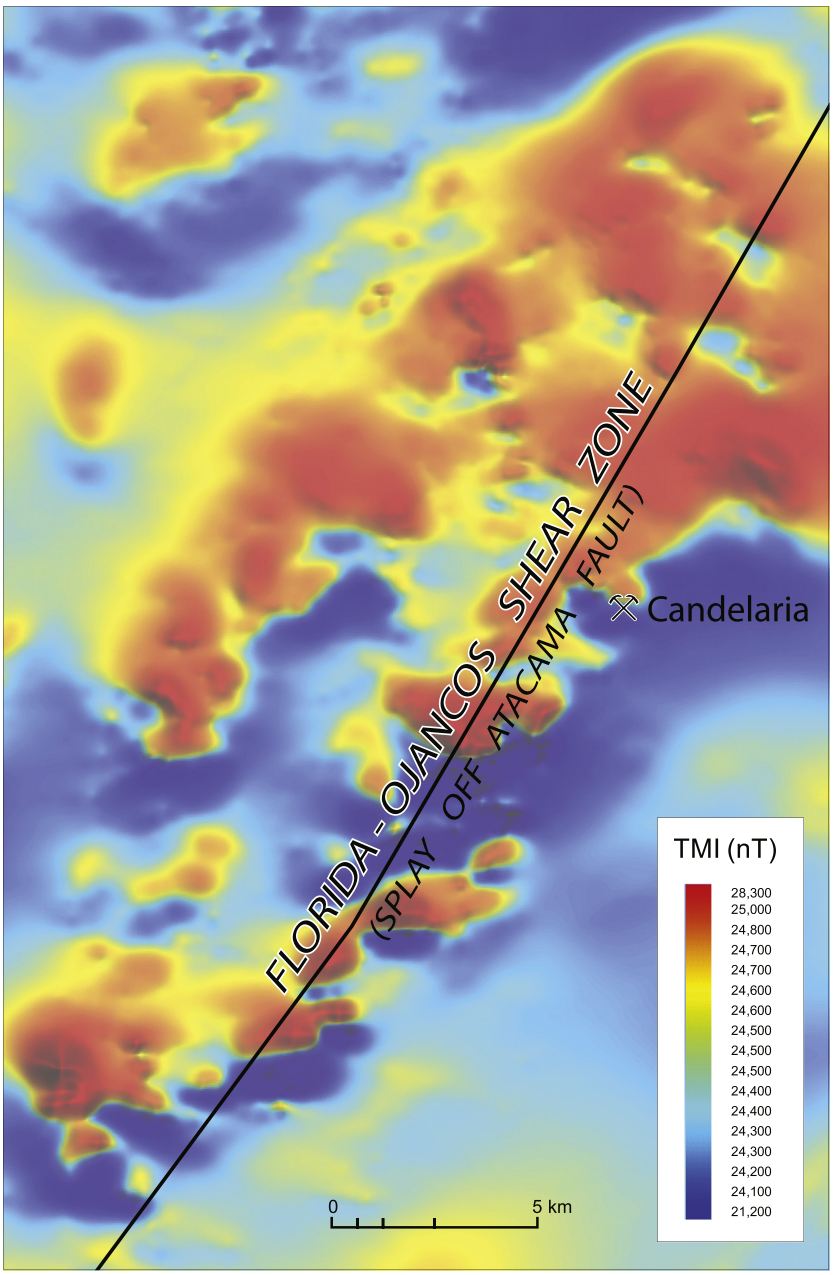

Fig. 13. A TMI image showing the repetition of NNE–SSW aligned anomalies adjacent to the Florida-Ojancos Shear Zone. Data courtesy of Fugro Gravity and Magnetic Services, Inc.

Graef, 2003; Hillan, 2013a). A simpler model of the Candelaria anomaly is constructed as a collection of 4 sub-horizontal, highly susceptible (3–4 SI) sheets. The models are discretised in a 3D volume with a resolution of 10 m for a cubic side length, and the magnetizations and TMI fields computed both with and without demagnetization corrections.

Fig. 16 plots the total magnetization as a north–south section through the bodies, both without (Fig. 16A) and with (Fig. 16B) the demagnetising effects included. In the bottom panel there is considerable spatial variation in the magnetization, but on average it has been suppressed by the order of tens of A/m. Some of the variation is due to the real interactions between the sheets and some is an artefact of the volume discretisation which introduces 'steps' into the model. The latter may be improved by refining the resolution of the discretisation.

Fig. 17 plots the TMI grid forward computed from the two cases both without (Fig. 17A) and with (Fig. 17B) the demagnetization effects. The TMI images show considerable suppression of the anomalies, more so of the positive anomalies, due to the complex interactions and magnetization suppression illustrated in Fig. 16B. The anomaly with demagnetization effects included appears as though the inducing field has rotated to a shallower inclination and a very slight rotation clockwise. This difference between the TMI grids is explicitly calculated and plotted in Fig. 18, which highlights the large suppression (as much as 1000 nT; 50% reduction of magnetic intensity)) of the positive anomalies just north of the main magnetic low (referring to the anomalies in Fig. 17). In this way the layered sheet model naturally gives rise to what appears to be a positive anomaly flanked to the north and south by magnetic lows without the need to invoke any remanent magnetization component.

These experiments demonstrate that the complexity of the Candelaria anomaly can be modelled by complex interactions of self-demagnetising bodies within the layered, "manto" style architecture (e.g., Marschik and Fontboté, 2001) that is typical of this area (e.g., Sillitoe, 2003). We furthermore interpret that the clockwise rotation of the anomaly axis, attributed to remanence by Taylor (2000), is instead due to these complex

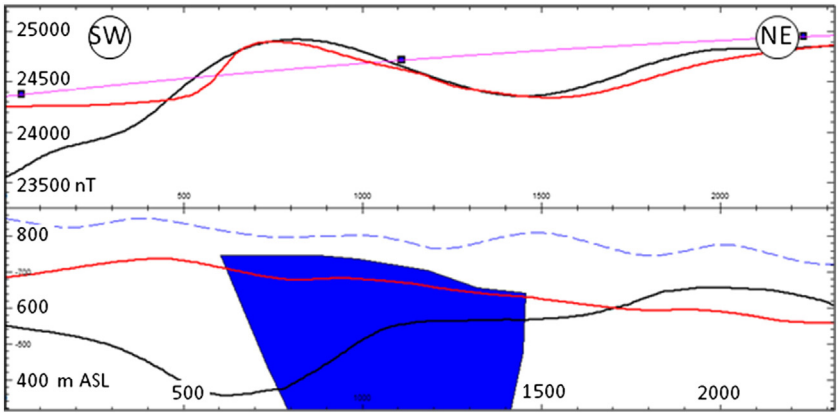

Fig. 14. A replication of the magnetic modeling of Taylor (2000). Upper window: Pink line = regional gradient; Red = modeled TMI; Black = measured TMI. Lower window: Dashed blue line = Sensor height; Red = pre-mining ground surface; Black = current surface. The body in blue has a susceptibility of 0.005 cgs (0.063 SI) and a Koenigsberger ratio of ~5. The remanence is "assumed" to have a declination of 215° and inclination of 40°. (For interpretation of the references to colour in this figure legend, the reader is referred to the web version of this article.)

interactions, probably coupled with incomplete separation of residual from regional anomalies.

8. Conclusions

Magnetite-rich end members of the IOCG family (e.g., Candelaria, Osborne, Starra, Ernest Henry, Brumby) have high susceptibilities, but because they contain such high proportions of coarse-grained magnetite the remanent magnetization within them is commonly multidomain (i.e., "soft"; easily reset). Therefore magnetite-rich IOCGs do not commonly retain large components of stable remanent magnetization oblique to the Earth's local field, but, due to their high susceptibility, are commonly affected by self-demagnetization.

This conclusion is confirmed for the magnetization of the Candelaria orebody, which is predominantly induced, refuting earlier suggestions (e.g., Taylor, 2000) that the associated magnetic anomaly is dominated by remanence (as was also noted by Roperch et al., 2001). Where there is significant remanent magnetisation it would be appropriate to incorporate both remanence and magnetic susceptibility to determine a bulk magnetisation intensity and inclination (e.g., Austin and Foss, 2014). However in this case, because remanence is so weak, we have simply calculated a mean magnetic susceptibility value for the lithologies sampled. The average susceptibility of the orebody samples is 3.4 SI, reflecting the high magnetite content of the Candelaria mineralisation. Within the ore rocks there is a spread of susceptibilities ranging from about 0.2 to 8 SI. Samples with >80% magnetite (e.g., Can 1 and Can 3)

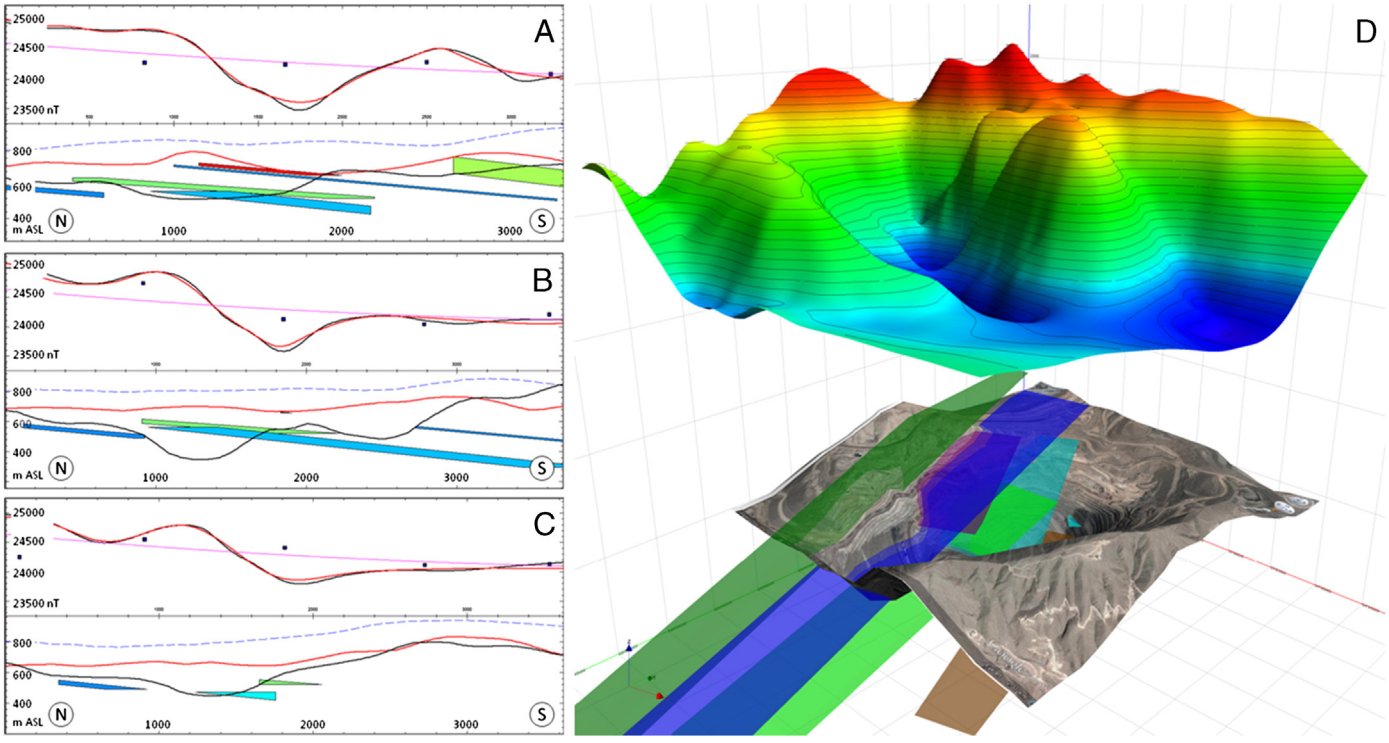

Fig. 15. A), B) and C) 3D Magnetic modeling along 3 sections (above) explain the anomaly at Candelaria well (rms error 3.2%) with a series of sub-parallel bodies of high susceptibility, dipping shallowly to the south. The bodies are colored by their susceptibility, with dark blue = 3 SI and red = 4 SI. Lines shown are as for Fig. 14. D) A 3D view of the modeling result showing total magnetic intensity (top; data supplied by Fugro Gravity and Magnetic Services Inc.) above a GoogleEarth™ image which is draped over SRTM data (below). The modeled bodies are shown stepping up to the west through the pit. NB: in Figs. A–C that the sub-horizontal magnetite bodies correspond to areas that have been mined out, indicating that the model is a good approximation of the magnetic architecture of the deposit.

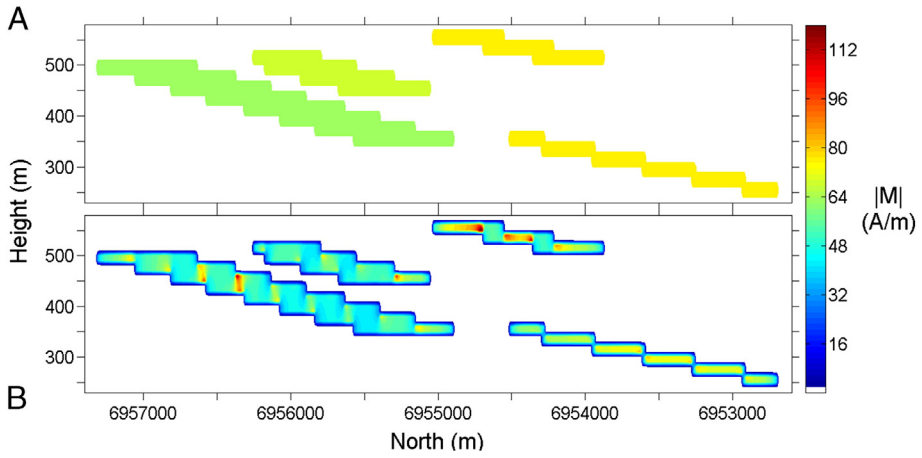

Fig. 16. North–south cross sections, through 372500 (m) east, showing the total magnetization distribution through the modeled bodies and host rock. The total magnetization is plotted both: A) without the demagnetising effect incorporated and; B) with the demagnetising effect incorporated. NB: There is an approximately 5× vertical exaggeration.

sit at the higher end of this range 4–8 SI and are modelled as magnetite-rich mantos, whilst ore rocks with lesser amounts of magnetite have much lower values (e.g., 0.2–2 SI). For the purposes of modelling, we used values of 3–4 SI for modelling the magnetite-rich mantos. Altered host rock samples adjacent to the orebody have an average susceptibility of 0.12 SI and diorite samples from surface exposures of the batholith have much lower average susceptibility (~0.04 SI). For the purposes of modelling, these rocks are essentially non-magnetic, and we accounted for them in setting the background field.

Although relatively weak (<10% of the induced magnetization), remanent magnetisation of both polarities is recorded by the rocks and ores of the Candelaria area. The dominant normal polarity component is NE and up. This component is interpreted as mid-Cretaceous: primary in the case of the diorites; secondary, associated with magnetite (and minor pyrrhotite) alteration, in the Candelaria sequence. The subordinate reverse polarity direction is antipodal: SW down. This is interpreted as an overprint related to a low grade thermal event or weak alteration event that is considerably younger (<83 Ma) than the mid-Cretaceous Candelaria mineralisation.

Palaeomagnetic directions indicate clockwise rotation of the Candelaria area, including the nearby batholith, through at least 45° since the mid-late Cretaceous. This rotation is recorded by reverse polarity directions as well as normal polarity remanence, indicating that it occurred post 83 Ma. This conclusion confirms the suggestion of Taylor (2000) that the area had undergone clockwise rotation, based partly on the NE–SW orientation of the axis of a local dipolar magnetic anomaly at Candelaria. Furthermore, the results are consistent with regional paleomagnetic studies e.g., Arriagada et al. (2000, 2003).

Modelling of the Candelaria anomaly in its regional context was constrained by its measured magnetic properties, and modelled using the self-demagnetization setting in ModelVisionPro™. The final magnetic model consisted of numerous sub-horizontal sheets (dipping ~5° south) with magnetic susceptibilities of 3–4 SI, which are truncated by a series of N–S faults. The magnetite sheets are inverted about the fault, resulting in the west over east displacement of the magnetite sheets.

There are considerable differences between the observed fields when demagnetising effects are included in forward modelling. We have shown differences of up to 1000 nT (50% reduction of magnetic intensity) arising from the complex demagnetising and interaction effects causing suppression of the internal fields and minor rotation of the magnetization vector into the plane of the magnetite sheets.

It must be noted that any number of models could be used to explain a given anomaly, in the absence of geological and petrophysical constraints, due to the inherent non-uniqueness of magnetic modelling. However, this work shows that it is imperative to consider the effects of remanence and self-demagnetization to achieve accurate geophysical modelling of magnetite-rich iron oxide Cu–Au systems. Using geological and magnetic property information to constrain modelling, we have produced a robust explanation for the complex Candelaria magnetic anomaly pattern, without invoking strong remanent magnetization

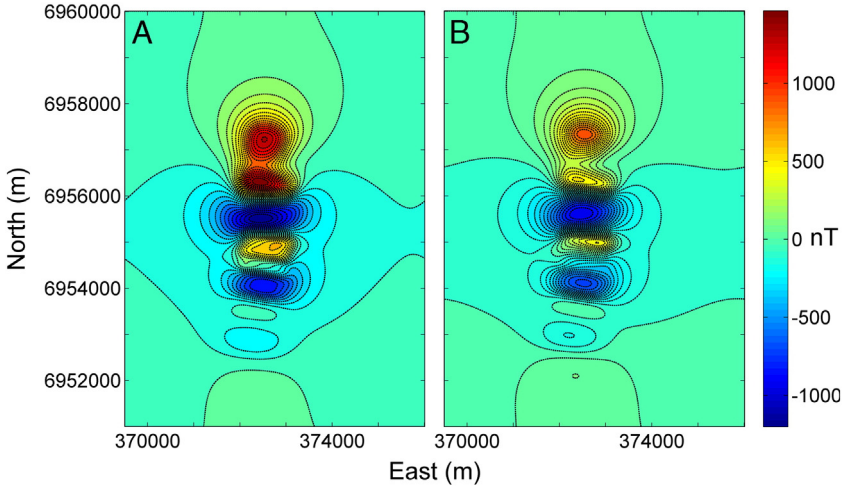

Fig. 17. Contoured TMI images calculated from the synthetic model at 800 m altitude. A) Shows the anomaly from the bodies as modelled and; B) shows anomaly from the bodies after the demagnetising effect has been incorporated.

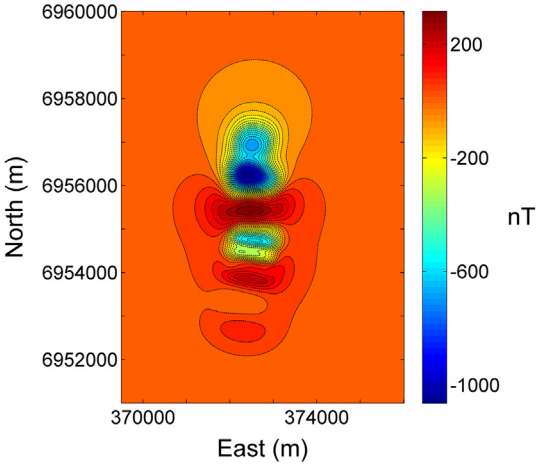

Fig. 18. Contour plot of the difference between the TMI grids in Fig. 17. Areas where fields have become more negative are plotted as cooler colours, while areas where fields have become more positive are plotted as warmer colours.

via the accurate modelling of self-demagnetisation and complex magnetic interactions between bodies.

Acknowledgements

We thank Fugro (now CGG) Gravity and Magnetic Services Inc. for providing the magnetic data utilized in this study. Sampling of the Candelaria deposit and environs was undertaken as part of AMIRA International project P700. We thank Walter Martin of Compañía Contractual Minera Candelaria for access to the deposit. Thanks to our colleagues in the Magnetics and Gravity team at CSIRO: Phil Schmidt, Clive Foss, and Mike Tetley, for their assistance and encouragement on this project. The first author would particularly like to thank Mike McWilliams for the opportunity to present this work in South America and visit some of its many porphyries and IOCGs.

References

Aharoni, A., 1998. Demagnetizing factors for rectangular ferromagnetic prisms. J. Appl. Phys. 83 (6).
Arévalo, C., 1999. The Coastal Cordillera-Precordillera boundary in the Copiapó area, northern Chile and the structural setting of the Candelaria Cu-Au ore deposit: Unpublished Ph.D. thesis, Kingston-Upon-Thames, Kingston University, 244 pp.
Arévalo, C., Grocott, J., 1997. The tectonic setting of the Chañarcillo Group and the Bandurrias Formation: An Early-Late Cretaceous sinistral transpressive belt between the Coastal Cordillera and the Precordillera, Atacama region, Chile: Congreso Geológico Chileno, 8th, Antofagasta, 1997. Actas 1604–1607.
Arévalo, C., Grocott, J., Martin, W., Pringle, M., Taylor, G., 2006. Structural Setting of the Candelaria Fe Oxide Cu-Au Deposit, Chilean Andes (27° 30′ S). Econ. Geol. 101 (4), 819–841.
Arriagada, C., Roperch, P., Mpodozis, C., 2000. Clockwise block rotations along the eastern border of the Cordillera de Domeyko, Northern Chile (22°45'-23°30'S). Tectonophysics 326, 153–171.
Arriagada, C., Roperch, P., Mpodozis, C., Dupont-Nivet, G., Cobbold, P.R., Chauvin, A., Cortés, J., 2003. Paleogene clockwise tectonic rotations in the forearc of central Andes, Antofagasta region, northern Chile. J. Geophys. Res. 108 (B1), 2032. http://dx.doi.org/10.1029/2001JB001598.
Astudillo, N., Roperch, P., Townley, B., Arriagada, C., Maksaev, V., 2010. Magnetic polarity zonation within the El Teniente copper-molybdenum porphyry deposit, central Chile. Mineral. Deposita 45, 23–41.
Austin, J.R., Foss, C.A., 2014. The Paradox of Scale: Reconciling magnetic anomalies with rock magnetic properties for cost-effective mineral exploration. J. Appl. Geophys. 104 (2014), 121–133.
Austin, J.R., Schmidt, P.W., Foss, C.A., 2013a. Magnetic modelling of Iron Oxide Copper-Gold mineralization constrained by 3-D multi-scale integration of petrophysical and geochemical data: Cloncurry District, Australia. Interpretation 1 (1), T63–T84.
Austin, J.R., Schmidt, P.W., Lilly, R., 2013b. Anisotropy of Magnetic Susceptibility (AMS) and Palaeomagnetism applied to the differentiation of structural and metallogenic controls on Iron Oxide Copper-Gold (IOCG) mineralization: a case study from Monakoff, NW Queensland. Extended Abstracts, 23rd Annual Australian Society of Exploration Geophysicists Conference and Exhibition, Melbourne.
Austin, J.R., Clark, D., Schmidt, P.W., Hillan, D., Foss, C.A., 2013c. Magnetic anomalies to mines: Practical insights into the myths, methods and mysteries in relating mineralisation and magnetisation. Remanence and Demagnetisation Forum, 23rd Annual Australian Society of Exploration Geophysicists Conference and Exhibition, Melbourne.
Austin, J.R., Hillan, D., Schmidt, P.W., Foss, C.A., 2014. Giles, complex, magnetism. *Abstracts*, Australian Earth Science Convention, July 7-10 2014, Newcastle, Australia.
Beck Jr., M.E., Burmester, R.F., Craig, D.E., Grommé, C.S., Wells, R.E., 1986. Paleomagnetism of the middle Tertiary volcanic rocks from the Western Cascade Series, northern California. J. Geophys. Res. 91, 8219–8230.
Beleggia, M., De Graef, M., 2003. On the computation of the demagnetization tensor field for an arbitrary particle shape using a Fourier space approach. J. Magn. Magn. Mater. 263, L1–L9.
Bookstrom, A.A., 1977. The magnetite deposits of El Romeral, Chile. Econ. Geol. 72, 1101–1130.
Butler, 1992. Paleomagnetism: Magnetic Domains to Geologic Terranes. Blackwell Scientific Publications.
Camus, F., 1980. Posible modelo genético para los yacimientos de cobre del distrito minero Punta del Cobre. Rev. Geol. Chile 11, 51–76.
Clark, D.A., 1988. Magnetic Properties and Magnetic Signatures of the Trough Tank and Starra Copper-Gold Deposits, Eastern Mount Isa Block: AMIRA Project 78/P96B: Applications of Rock Magnetism.
Clark, D.A., 1994. Magnetic properties and magnetic contents of ores from the Ernest Henry Deposit, Eastern Mount Isa Inlier. CSIRO Exploration and Mining, Report 23C.
Clark, D.A., 2000. Self-demagnetisation in practice: the Osborne Cu-Au deposit. Preview 85, 31–36.
Clark, D.A., 2014. Magnetic effects of hydrothermal alteration in porphyry copper and iron-oxide copper–gold systems: A review. Tectonophysics 624–625, 46–65.
Clark, D., Emerson, D., 1999. Self-demagnetization. Preview (ASEG) 79, 22–25.
Clark, D.A., Lackie, M.A., 2003. Palaeomagnetism of the Early Permian Mount Leyshon Intrusive Complex and Tuckers Igneous Complex, North Queensland, Australia. Geophys. J. Int. 153, 523–547.
Clark, D., Schmidt, P., 1994. Magnetic properties and magnetic signatures of BIFs of the Hamersley Basin and Yilgarn block. Western Australia: Geophysical Signatures of Western Australian Mineral Deposits,pp. 343–354.
Clark, D.A., Geuna, S., Schmidt, P.W., 2003. Predictive Magnetic Exploration Models for Porphyry. Epithermal and Iron Oxide Copper-Gold Deposits: Implications for Exploration, Exploration and Mining: AMIRA Report 1073R.
Dallmeyer, R.D., Brown, M., Grocott, J., Taylor, G.K., Treloar, P.J., 1996. Mesozoic Magmatic and Tectonic Events within the Andean Plate Boundary Zone, 26°-27°30'S, North Chile: Constraints from Mineral Ages. J. Geol. 104 (1), 19–40.
Day, R., Fuller, M., Schmidt, V.A., 1977. Hysteresis properties of titanomagnetites: Grain-size and compositional dependence. Phys. Earth Planet. Inter. 13 (4), 260–267.
Dunlop, D.J., Özdemir, Ö., 1997. Rock Magnetism: Fundamentals and Frontiers. Cambridge University Press, (573 pp.).
Ellis, R.G., de Wet, B., Macleod, I.N., 2012. Inversion of Magnetic Data from Remanent and Induced Sources. 22nd Annual Australian Society of Exploration Geophysicists Conference and Exhibition, Brisbane (Electronic Abstracts).
Espinoza, S., 1990. The Atacama-Coquimbo ferriferous belt, northern Chile. Society for Geology Applied to Mineral Deposits Special Publication. 8, pp. 395–412.
Gay, S.P., 1963. Standard curves for interpretation of magnetic anomalies over long tabular bodies. Geophysics 28, 161–200.
Geuna, S.E., Somoza, R., Vizán, H., Figari, E., Rinaldi, C., 2000. Paleomagnetism of Jurassic and Cretaceous rocks in Central Patagonia: a key to constrain the timing of rotations during the breakup of southwestern Gondwana? Earth Planet. Sci. Lett. 181, 145–160.
Gidley, P.R., 1988. Geophysics of the Trough Tank Gold-Copper prospect, Australia. Bull. Aust. Soc. Explor. Geophys. 19, 76–78.
Guo, W., Dentith, M., Zhengxiang, L., Powell, C., 1998. Self demagnetization corrections in magnetic modelling: some examples. Explor. Geophys. 29, 396–401.
Guo, W., Dentith, M., Bird, R., Clark, D., 2001. Systematic error analysis of demagnetization and implications for magnetic interpretation. Geophysics 66, 562–570.
Hayward, N., Enkin, R.J., Corriveau, L., Montreuil, J.F., Kerswill, J., 2013. The application of rapid potential field methods for the targeting of IOCG mineralisation based on physical property data, Great Bear magmatic zone, Canada. J. Appl. Geophys. 94, 42–58.
Hillan, D., 2013a. Modelling Self-Demagnetization and Body-Body Interactions in the Fourier Domain: EAGE 2013 Extended Abstract. ,pp. 1–4.
Hillan, D., 2013b. Self-demagnetization: implications and corrections in magnetic modelling. A Forum on the Application of Remanent Magnetization and Self-Demagnetization Estimation to Mineral Exploration 23rd ASEG Conference and Exhibition, Melbourne.
Hopf, S., 1990. The Agustina mine, a volcanic-hosted copper deposit in northern Chile. Soc. Geol. Appl. Miner. Depos. Spec. Publ. 8, 421–434.
Jurgan, H., 1977. Strukturelle und lithofazielle Entwicklung des andinen Unterkreide-Beckens im Norden Chiles (Provinz Atacama). Geotekt. Forsch. 52 (138 pp.).
Krahenbuhl, R.A., Li, Y., 2007. Influence of self-demagnetization effect on data interpretation in strongly magnetic environments. ,pp. 713–717, (SEG 2007 Extended Abstracts).
Marschik, R., Fontboté, L., 1996. Copper(-iron) mineralization and superposition of alteration events in the Punta del Cobre belt, northern Chile. Society of Economic Geologists Special Publication. 5, pp. 171–189.
Marschik, R., Fontboté, L., 2001. The Candelaria-Punta del Cobre iron oxide Cu-Au (-Zn-Ag) deposits, Chile. Econ. Geol. 96, 1799–1826.
Marschik, R., Leveille, R.A., Martin, W., 2000. La Candelaria and the Punta del Cobre district, Chile: Early Cretaceous iron oxide Cu-Au(-Zn-Ag) mineralization. In: Porter, T.M. (Ed.), Hydrothermal iron-oxide copper gold & related deposits: A global perspective: Adelaide, Australian Mineral Foundation, pp. 163–175.
Ridley, B.H., Brown, H.E., 1980. The transformer bridge and magnetic susceptibility measurements. Bull. Aust. Soc. Explor. Geophys. 11, 110–114.
Roperch, P., Tassara, A., Townley, B., 2001. Discussion on ``Palaeomagnetism applied to magnetic anomaly interpretation: a new twist to the search for mineralisation in

northern Chile" by Taylor (Mineralium Deposita v. 35: p. 377-384, 2000). Mineral. Deposita 36, 195–196.
Ryan, P.J., Lawrence, A.L., Jenkins, R.A., Matthews, J.P., Zamora, J.C., Marino, E., Urqueta, I., 1995. The Candelaria copper-gold deposit, Chile. Ariz. Geol. Soc. Dig. 20, 625–645.
Sandrin, A., Elming, S.-Å., 2006. Geophysical and petrophysical study of an iron oxide copper gold deposit in northern Sweden. Ore Geol. Rev. 29 (1), 1–18.
Scheuber, E., Hammerschmidt, K., Friedrichsen, H., 1995. 40Ar/39Ar and Rb-Sr analyses from ductile shear zones from the Atacama fault zone, northern Chile: The age of deformation. Tectonophysics 250, 61–87.
Schmidt, P.W., 1982. Linearity spectrum analysis of multicomponent magnetizations and its application to some igneous rocks from south-eastern Australia. Geophys. J. R. Astron. Soc. 79, 647–665.
Schmidt, P.W., 1993. Palaeomagnetic cleaning strategies. Phys. Earth Planet. Inter. 76 (1–2), 169–178.
Schmidt, P.W., Clark, D.A., 1994. Palaeomagnetism and magnetic anisotropy of Proterozoic banded-iron formations and iron ores of the Hamersley Basin, Western Australia. Precambrian Res. 69, 133–155.
Segerstrom, K., Parker, R.L., 1959. Cuadrángulo Cerrillos, Provincia de Atacama. Carta Geológica de Chile. 1. Instituto de Investigaciones Geológicas, Santiago, (33 pp.).
Sillitoe, R.H., 2003. Iron oxide-copper-gold deposits: an Andean view. Mineral. Deposita 38, 787–812.
Sillitoe, R.H., Clark, A.H., 1969. Copper and copper iron sulphides as the initial products of supergene oxidation: Copiapó mining district, northern Chile. Am. Mineral. 54, 1684–1710.
Taylor, G.K., 2000. Palaeomagnetizm applied to magnetic anomaly interpretation; a new twist to the search for mineralisation in northern Chile. Mineral. Deposita 35, 377–384.
Thiele, R., Pincheira, M., 1987. Tectonica transpresiva y movimiento de desgarre en el segmento sur de la zona de Falla Atacama, Chile. Rev. Geol. Chile 31, 77–94.
Tilling, R., 1962, Batholith emplacement and contact metamorphism in the Paipote-Tierra Amarilla area, Atacama province, Chile: Unpublished Ph.D. thesis, New Haven, Connecticut, Yale University, 195 pp.
Tilling, R., 1963. Disequilibrium skarns of the Tierra Amarilla aureole, Atacama province, Chile [abs.]. Geol. Soc. Am. Spec. Pap. 76, 167.
Tilling, R., 1976. El Batolito Andino cerca de Copiapó, Provincía de Atacama. Geol. Petrol.: Rev. Geol. Chile 3, 1–24.
Townley, B., Roperch, P., Oliveros, V., Tassara, A., Arriagada, C., 2007. Hydrothermal alteration and magnetic properties of rocks in the Carolina de Michilla stratabound copper district, northern Chile. Mineral. Deposita 42, 771–789.
Zentilli, M., 1974, Geological evolution and metallogenetic relationships in the Andes of northern Chile between 26° and 29° S: Unpublished Ph.D. thesis, Kingston, Ontario, Queen's University, 394 pp.
Zietz, I., Henderson, R.G., 1956. A preliminary report on model studies of magnetic anomalies of three-dimensional bodies. Geophysics 21, 794–814.